



Article

Molybdenum Carbide Anchored on N,S Co-Doped Carbon Composite Derived from Lignosulfonate as a High Performance Electrocatalyst for Hydrogen Evolution Reaction

Na Yeong Oh¹, So Young Park¹, Ji Young Hwang¹, Hyung Mo Jeong² , Yong Sik Kim^{3,*} and Duck Hyun Youn^{1,*}

¹ Department of Chemical Engineering, Department of Integrative Engineering for Hydrogen Safety, Kangwon National University, Chuncheon 24341, Korea

² School of Mechanical Engineering, Department of Smart Fab. Technology, Sungkyunkwan University, Suwon 16419, Korea

³ Department of Paper Science & Engineering, Kangwon National University, Chuncheon 24341, Korea

* Correspondence: yongsikk@kangwon.ac.kr (Y.S.K.); youndh@kangwon.ac.kr (D.H.Y.)

Abstract: A composite of Mo₂C nanoparticles dispersed onto a nitrogen and sulfur co-doped carbon scaffold (Mo₂C/N,S-C) was prepared by a simple and environmentally friendly method of one-pot annealing of MoCl₅, urea, and lignosulfonate under a N₂ atmosphere at 700 °C. Lignosulfonate, a by-product of the sulfite pulping process, was employed as a feedstock to fabricate the S-doped carbon scaffold and carbide simultaneously, and urea acted as a nitrogen source for N-doping to carbon. The as-prepared Mo₂C/N,S-C catalyst showed high performance for the hydrogen evolution reaction (HER), with a small overpotential of 105 mV at 10 mAcm⁻², and good stability for 3000 cycles. The improved HER performance of the Mo₂C/N,S-C originated from the interplay between the highly active Mo₂C nanoparticles and the N,S co-doped carbon scaffold with its high electrical conductivity and large surface area. Furthermore, N,S co-doping to carbon improved the hydrophilicity of the catalyst surface, thus further enhancing the HER activity.

Keywords: electrocatalyst; hydrogen evolution reaction; lignosulfonate; molybdenum carbide; N,S co-doped carbon



Citation: Oh, N.Y.; Park, S.Y.; Hwang, J.Y.; Jeong, H.M.; Kim, Y.S.; Youn, D.H. Molybdenum Carbide Anchored on N,S Co-Doped Carbon Composite Derived from Lignosulfonate as a High Performance Electrocatalyst for Hydrogen Evolution Reaction. *Nanomaterials* **2022**, *12*, 3047. <https://doi.org/10.3390/nano12173047>

Academic Editor: Antonino Gulino

Received: 9 August 2022

Accepted: 28 August 2022

Published: 2 September 2022

Publisher's Note: MDPI stays neutral with regard to jurisdictional claims in published maps and institutional affiliations.



Copyright: © 2022 by the authors. Licensee MDPI, Basel, Switzerland. This article is an open access article distributed under the terms and conditions of the Creative Commons Attribution (CC BY) license (<https://creativecommons.org/licenses/by/4.0/>).

1. Introduction

Increasing energy consumption and environmental pollution have prompted the development of clean and renewable energy sources for the alleviation of human dependence upon exhaustible fossil fuels [1,2]. Hydrogen is recognized as an alternative energy source as it is abundant, clean, and energy-dense. Water electrolysis powered by renewable electricity is one of the most environmentally benign and sustainable hydrogen production technologies [3–5]. A hydrogen evolution reaction (HER) is the cathodic reaction of water electrolysis, wherein Pt is the most efficient electrocatalyst due to the negligible overpotential provided by the appropriate hydrogen binding energy of its surface [6]. However, the high cost and finite reserves of Pt limit large-scale application of water electrolysis. Therefore, the development of noble-metal-free electrocatalysts is of great importance [7,8].

Various molybdenum-based catalysts, including carbides (Mo₂C) [9,10], sulfides (MoS₂) [11,12], nitrides (Mo_xN, Ni₂Mo₃N) [13,14], and phosphides (MoP) [15], have proven their good HER activity as possible replacements for Pt. In particular, molybdenum carbides are attracting tremendous attention due to their high activity and stability for HER from their Pt-like electronic structure, high electrical conductivity, and high chemical stability [16,17]. Since Vrabel and Hu revealed that commercial Mo₂C possesses HER activity in both acidic and alkaline media [18], extensive research has been carried out to enhance the HER performance of Mo₂C by fabricating nanostructured Mo₂C catalysts and their composites with carbonaceous materials [19–26].

Next to cellulose, lignin is the second most abundant biopolymer and is generated as a by-product of the pulping process [27,28]. The lignin becomes sulfated during the sulfite pulping process, and the lignosulfonate is produced as a cross-linked polyphenolic polymer that contains sulfonic acid groups [29]. In contrast to hydrophobic lignin, lignosulfonate is an amphiphilic biopolymer and, as such, is soluble in water [30]. Small portions of produced lignosulfonate have been used as surfactants and adsorbents; however, most of it is unutilized and combusted for disposal producing carbon dioxide [31]. Thus, the effective utilization of lignosulfonate is required and inspired by its high carbon content and the presence of sulfur, we regard it as a suitable feedstock for the simultaneous fabrication of heteroatom-doped carbon and carbide.

Herein, sulfur and nitrogen co-doped carbon scaffolds decorated with molybdenum carbide nanoparticles ($\text{Mo}_2\text{C}/\text{N,S-C}$) were fabricated via the one-step pyrolysis of MoCl_5 , urea, and lignosulfonate at $700\text{ }^\circ\text{C}$ under N_2 flow for HER. During the synthesis, lignosulfonate plays critical roles as a source of sulfur for S-doping to carbon, and a source of carbon for the formation of amorphous carbon scaffold and carbide. At the same time, urea was employed as a nitrogen source for N-doping to carbon. Indeed, molybdenum carbide nanoparticles on S-doped carbon ($\text{Mo}_2\text{C}/\text{S-C}$) was fabricated without urea. The resultant $\text{Mo}_2\text{C}/\text{N,S-C}$ catalysts exhibited excellent HER activity in alkaline solution with a low overpotential value of 105 mV at 10 mA cm^{-2} , which is better than $\text{Mo}_2\text{C}/\text{S-C}$ and commercial Mo_2C (c- Mo_2C). Furthermore, the $\text{Mo}_2\text{C}/\text{N,S-C}$ showed good stability for 3000 cycles. The enhanced HER performance of $\text{Mo}_2\text{C}/\text{N,S-C}$ is due to the interplay between highly active Mo_2C nanoparticles and N,S-C scaffold providing high surface area and electrical conductivity. In addition, the enhanced HER performance of $\text{Mo}_2\text{C}/\text{N,S-C}$ is assisted by the improved hydrophilicity of the N,S-C scaffold relative to S-C scaffold. The high electrocatalytic performance and the simple and environmentally friendly synthetic method suggest that the $\text{Mo}_2\text{C}/\text{N,S-C}$ could be a promising catalyst for HER.

2. Materials and Methods

2.1. $\text{Mo}_2\text{C}/\text{N,S-C}$ Synthesis

An amount of 160 mg lignosulfonate (Aldrich, Pittsburgh, PA, USA) was dissolved in 15 mL ethanol under magnetic stirring. One gram of MoCl_5 (Alfa aesar, Haverhill, MA, USA) was dispersed in 2.53 mL ethanol and added to the lignosulfonate solution under vigorous stirring for 30 min. Then, 109.9 mg urea was added as a nitrogen source, with a molar ratio (R) of 0.5 with respect to Mo and stirred for 1 h. After drying the solution in an oven at $100\text{ }^\circ\text{C}$ for 90 min, the resultant mixture was annealed at $700\text{ }^\circ\text{C}$ ($3\text{ }^\circ\text{C min}^{-1}$ ramp) for 3 h under a N_2 atmosphere. As a control experiment, molybdenum carbide on a S-doped carbon ($\text{Mo}_2\text{C}/\text{S-C}$) catalyst was prepared by an identical method, except that 250 mg lignosulfonate was employed without the addition of urea. The weight contents of Mo_2C were measured as 35~40 wt.% for both the $\text{Mo}_2\text{C}/\text{N,S-C}$ and $\text{Mo}_2\text{C}/\text{S-C}$ samples.

2.2. Catalyst Characterization

Field-emission transmission electron microscopy (FE-TEM, JEOL, Akishima, Japan, JEM-2100F) and field-emission scanning electron microscopy (FE-SEM, JEOL, JSM-7900F) with energy dispersive X-ray spectrometer (EDS) were used to analyze morphologies and elemental compositions of the prepared samples. X-ray diffraction (XRD, Rigaku, Tokyo, Japan, MiniFlex 600) was conducted with $\text{Cu K}\alpha$ (1.54 \AA) radiation. X-ray photoelectron spectroscopy (XPS, Thermo-Scientific, Waltham, MA, USA, K-alpha) was used to investigate the chemical states of samples. The obtained binding energy values were calibrated by referencing the C 1s peak at 284.4 eV. The specific surface area and corresponding pore size distribution were investigated by measuring the N_2 adsorption–desorption isotherms at 77 K (Micromeritics, Norcross, GA, USA, ASAP 2020 PLUS). The contact angle measurements (Kruss, Kruss, Germany, Germany, DSA25) were conducted by loading the prepared catalysts (1 mg cm^{-2}) onto $1 \times 1\text{ cm}$ carbon paper (1 wt.% wet-proofing, Toray, Tokyo, Japan, TGP-H-060).

2.3. Electrochemical Tests

All of the electrochemical measurements were conducted on a three-electrode electrochemical workstation (PAR, VersaSTAT 4) equipped with a rotating disk electrode (RDE, PINE Research) in a 1 M KOH aqueous solution. To prepare the working electrode, 20 mg of prepared catalyst was dispersed in 2 mL water and then 20 μL catalyst ink was loaded onto a glassy carbon electrode (0.19635 cm^2). The reference and counter electrodes were Ag/AgCl (4 M KCl) electrode and Pt wire, respectively. All recorded potential values were converted to the reversible hydrogen electrode (RHE) with iR-compensation. Linear sweep voltammetry (LSV) curves were conducted at scan rate of 5 mV s^{-1} with 900 rpm. Electrochemical impedance spectra (EIS) were performed in the frequency range from 100 kHz to 0.1 Hz at 105 mV (vs. RHE) overpotential with 6 mV modulation amplitude. Stability tests of prepared electrocatalysts were obtained by repeating 3000 cycles with potential range of 0.2 V to -0.2 V (vs. RHE). Electrochemical double layer capacitances (EDLC) were conducted by cyclic voltammetry (CV) from 0.1 to 0.3 V (vs RHE) at various scan rates of 20, 60, 100, 140 and 180 mV s^{-1} .

3. Results and Discussion

The synthesis of the $\text{Mo}_2\text{C}/\text{N,S-C}$ catalyst is summarized in Scheme 1. Molybdenum chloride and urea was dissolved in ethanol solution containing the lignosulfonate and the subsequent annealing under N_2 at $700\text{ }^\circ\text{C}$ yielded $\text{Mo}_2\text{C}/\text{N,S-C}$. During the synthesis, urea acted as a nitrogen source and lignosulfonate acted as carbon and sulfur sources. Notably, $\text{Mo}_2\text{C}/\text{S-C}$ catalyst was generated without urea by an identical synthetic method, thereby demonstrating that that carbon sources from lignosulfonate played multiple roles in generating carbide and carbon scaffold at the same time. In addition, sulfur and nitrogen sources from lignosulfonate and urea served to S and N doping to carbon scaffold, respectively. The proposed synthetic method has the following advantages: (i) it is a simple method in which the formation of Mo_2C and the generation of amorphous carbon scaffold and N,S co-doping to the carbon scaffold are synchronously accomplished via mixing and annealing of the precursors in one pot, (ii) no toxic gases or chemicals were required for Mo_2C synthesis and N,S co-doping, (iii) the method is environmentally friendly due to the use of lignosulfonate, an industrial waste material, as a precursor, and (iv) our synthetic method produced Mo_2C nanoparticles with a size of ca. A total of 7 nm dispersed in N,S co-doped carbon scaffold ($\text{Mo}_2\text{C}/\text{N,S-C}$), which recorded one of the best performances for HER among the biomass-derived Mo_2C -based catalysts.



Scheme 1. Schematic illustration for the preparation of $\text{Mo}_2\text{C}/\text{N,S-C}$.

The SEM image of the $\text{Mo}_2\text{C}/\text{N,S-C}$ in Figure 1a reveals the presence of amorphous carbon clusters of $\sim 4\text{ }\mu\text{m}$ in size, while the corresponding EDS elemental mapping images in Figure 1b–e reveal the almost identical distributions of molybdenum, carbon, nitrogen, and sulfur, respectively, thereby indicating that the Mo_2C nanoparticles are uniformly distributed on the N,S co-doped carbon scaffold. In the TEM image (Figure 1f), the Mo_2C nanoparticles are dispersed on amorphous carbon composite with an average particle size of 7 nm. The HR-TEM and fast Fourier transform (FFT) images are shown in Figure 1g. The lattice spacings of 0.226 and 0.237 nm are assigned to Mo_2C (101) and (002) crystalline

planes, respectively (Figure 1g). In comparison, TEM images of Mo₂C/S-C were also presented in Figure S1. The Mo₂C nanoparticles are distributed on S-doped carbon scaffolds with a diameter of 16 nm. The lattice distance of 0.237 nm corresponds to the reflection of the (002) plane (Figure S1).

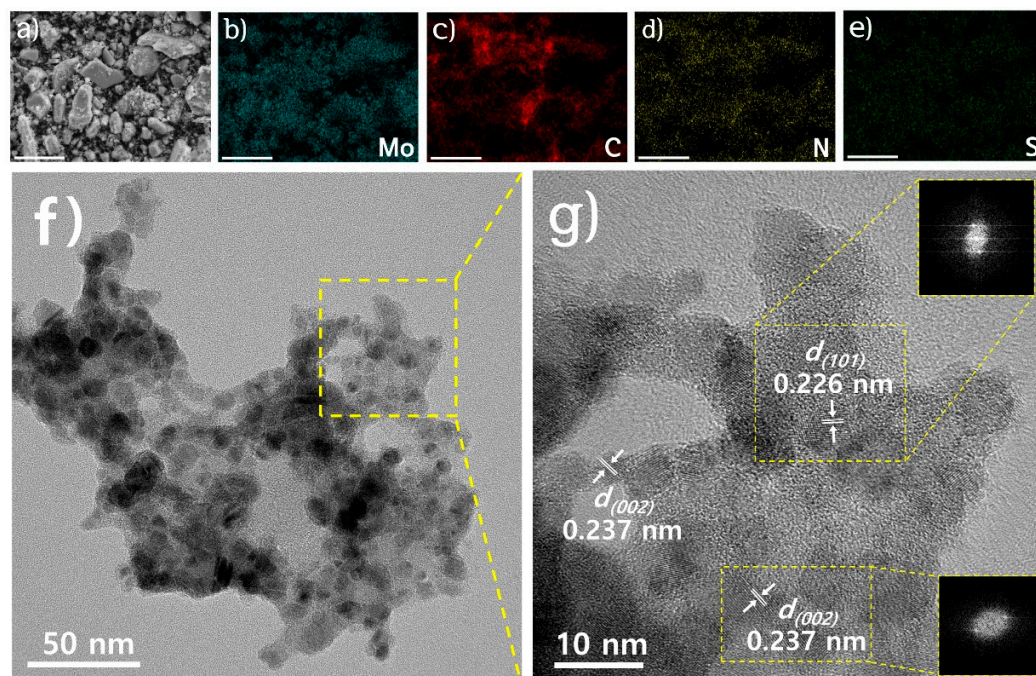


Figure 1. (a) SEM image of Mo₂C/N,S-C and corresponding SEM-EDS elemental mapping for (b) Mo, (c) C, (d) N, and (e) S (scale bar = 10 μm). (f) TEM and (g) HR-TEM images of Mo₂C/N,S-C. Insets in (g) denote FFT images.

Figure 2a shows the XRD patterns for the Mo₂C/N,S-C and Mo₂C/S-C catalysts, which are consistent with their hexagonal β-Mo₂C reference XRD patterns (JCPDS 00-035-0787). The peaks at 34.4°, 38.0°, 39.4°, 52.1°, 61.5°, 69.6°, 74.6°, 75.5°, 81.2° and 84.8° correspond to the (100), (002), (101), (102), (110), (103), (112), (201), (004), and (202) lattice planes, respectively. No impurity peaks were detected such as metallic molybdenum or molybdenum oxides for both catalysts.

The XPS survey spectrum for Mo₂C/N,S-C (Figure S2) confirmed the existence of molybdenum, nitrogen, carbon, and sulfur elements on the catalyst surface. The amounts of N and S in Mo₂C/N,S-C due to co-doping to carbon scaffold were determined to be 3.18 and 0.72 at.%, respectively, while Mo₂C/S-C (Figure S3a) contained 0.49 and 0.9 at.% of N and S. The elemental analysis results in Table S1 suggest that the N in the Mo₂C/S-C is derived from the lignosulfonate itself; however, the doping amount of N in Mo₂C/S-C is nearly 6.5 times lower than that in Mo₂C/N,S-C. The amounts of each element for Mo₂C/N,S-C and Mo₂C/S-C are summarized in Table S2.

In the high-resolution Mo 3d spectrum (Figure 2b), the peak deconvolution affirmed the existence of Mo₂C (Mo²⁺ at 228.25/231.4 eV), MoO₂ (Mo⁴⁺ at 229.2/232.8 eV), and MoO₃ (Mo⁶⁺ at 232.1/235.3 eV) [32–34]. The presence of oxides on the surface of the carbide material is unavoidable due to air exposure [9]. The N 1s spectrum in Figure 2c shows four peaks at 394.3, 397.1, 398.6, and 400.3 eV, corresponding to Mo 3p, pyridinic N, pyrrolic N, and graphitic N, respectively. There are two peaks at S 2p spectrum for Mo₂C/N,S-C shown in Figure 2d. The peaks at 161.5/162.68 eV were related sulfur doping to the carbon supports, and the peaks for oxidized S was determined at 163.6/169.6 eV [35,36]. The Mo 3d and S 2p spectra of Mo₂C/S-C were similar to those of Mo₂C/N,S-C (Figure S3b,d), thereby suggesting similar chemical states except for the much lower content of N element (Figure S3c).

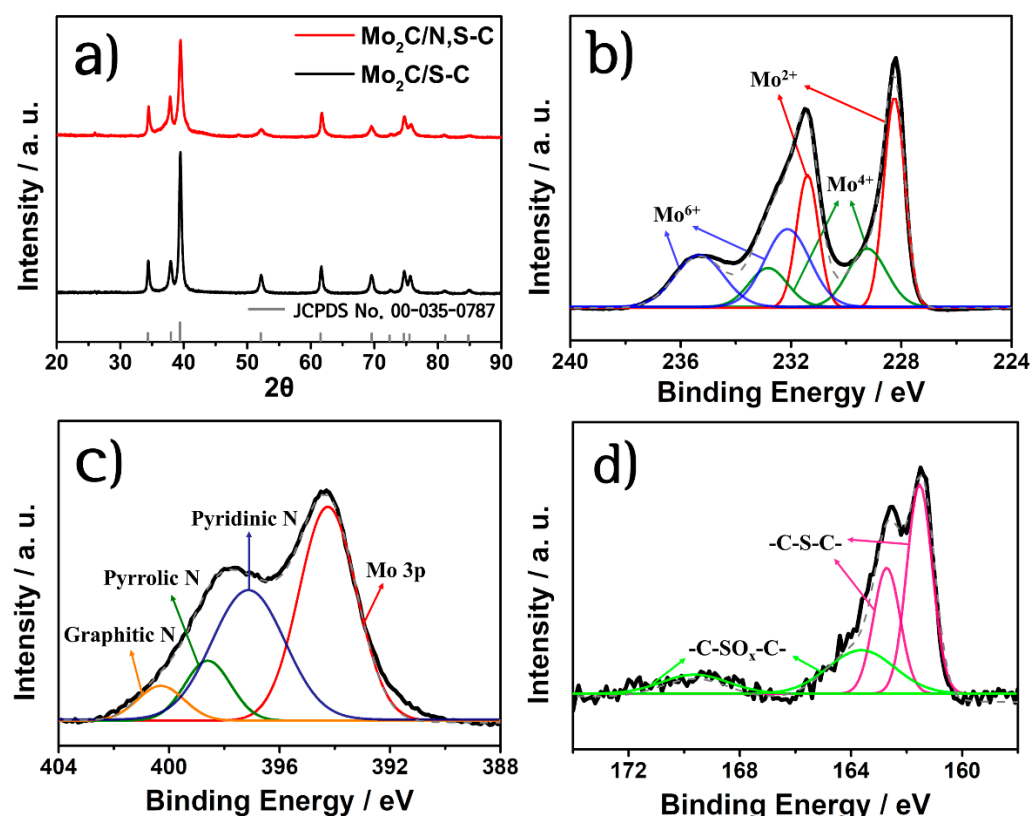


Figure 2. (a) XRD patterns of Mo₂C/N,S-C and Mo₂C/S-C. (b–d) High-resolution XPS spectra of Mo₂C/N,S-C for Mo 3d, N 1s and S 2p. Dotted lines denote raw data and other lines represent deconvoluted data.

The mesoporous texture of the Mo₂C/N,S-C was revealed by the nitrogen adsorption-desorption results shown in Figure S4a, which exhibit a type IV isotherm. The Brunauer–Emmett–Teller (BET) surface area of Mo₂C/N,S-C is 34.4 m² g^{−1} and the presence of mesopores was also verified by pore size distribution (PSD) using the Barrett–Joyner–Halenda (BJH) method (Figure S4b).

Figure 3a shows polarization curves for the prepared catalysts including Pt/C (20 wt.%, E-TEK) and commercial Mo₂C (c-Mo₂C) in 1M KOH solution. The Pt/C exhibited the best HER activity with small overpotential of 30 mV to drive 10 mA cm^{−2} (η_{10} value) [14]. By contrast, the c-Mo₂C with the η_{10} value of 225 mV is not suitable as a HER electrocatalyst which might be due to its largely aggregated particles and low electrical conductivity [18]. In contrast, the Mo₂C/S-C exhibited an improved HER activity with η_{10} value of 141 mV than c-Mo₂C, and this was significantly enhanced when the Mo₂C phases are combined with the N,S co-doped carbon scaffold, achieving a η_{10} value of 105 mV for the Mo₂C/N,S-C. This improved performance is comparable to that of the previously reported biomass-derived Mo₂C-based catalysts (Table S3). The coupling of Mo₂C with N,S-C scaffold not only prevented agglomeration of Mo₂C particles, but also provided high surface area and electrical conductivity [35]. In addition, the co-doping of N and S increases the charge and spin densities of carbon atoms compared to solely the doped carbon scaffolds, which results in a larger number of active carbon atoms [37]. Thereby, the N,S-C scaffold can further enhance the HER performance of Mo₂C by modulating the catalytic activity of carbon atoms adjacent to heteroatoms [38]. In addition, previous studies have demonstrated that multi-heteroatom doping increases the surface wettability of the electrocatalysts, thereby promoting their HER activity [39–42]. Hence, the increased activity of the Mo₂C/N,S-C relative to the Mo₂C/S-C is further explained in terms of the surface wettability of the catalysts in Figure 4. The water contact angles of the Mo₂C/N,S-C, Mo₂C/S-C, and c-Mo₂C are found to be 44°, 67°, and 85.3°, respectively, thereby demon-

strating that hydrophilicity was greatly enhanced by the introduction of N,S co-doped carbon scaffold. Hydrophilicity can facilitate the HER activity by lowering the adhesion force and facilitating the detachment of gas bubbles from the catalyst surface [35,43].

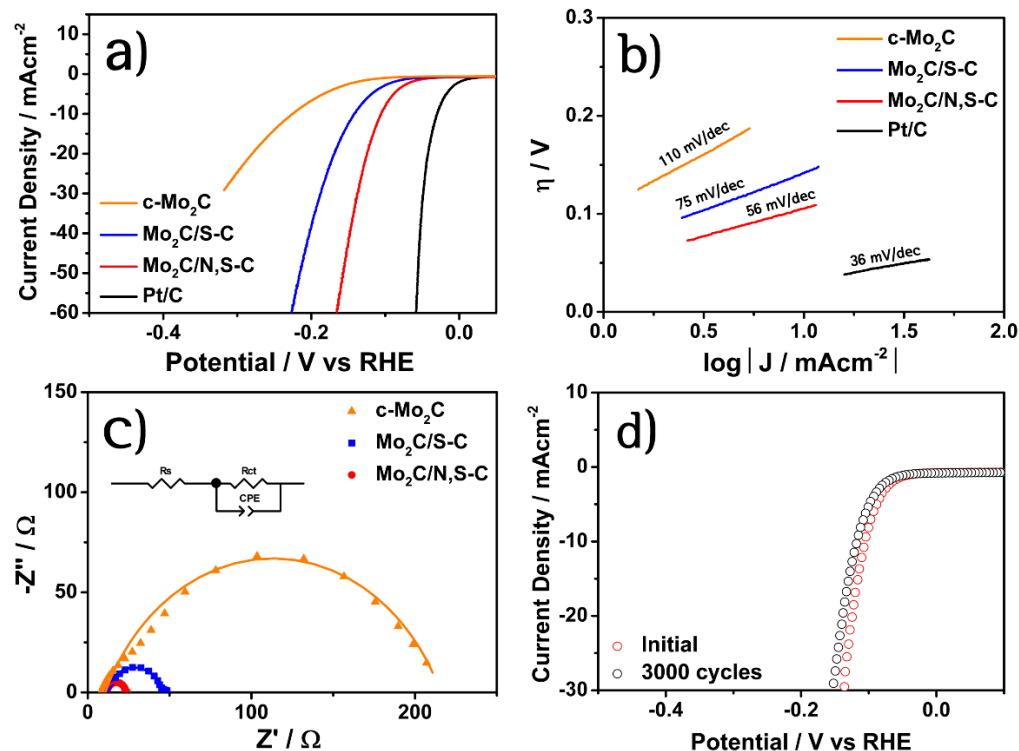


Figure 3. (a) Polarization curves of all prepared samples in 1 M KOH solution, (b) Tafel plots, (c) Nyquist plots with an equivalent circuit, and (d) stability tests of Mo₂C/N,S-C.

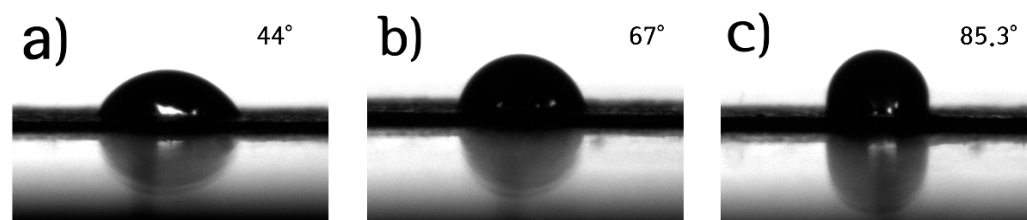


Figure 4. Contact angle measurement for (a) Mo₂C/N,S-C, (b) Mo₂C/S-C, and (c) c-Mo₂C.

Figure 3b shows the Tafel plots of the prepared catalysts, fitted to Tafel equation ($\eta = b \log |J| + a$, where b is the Tafel slope and J is the current density). The Tafel slope of Pt/C is 36 mV dec^{-1} , which is consistent with the previously reported value [20]. Meanwhile, the Tafel slope of the Mo₂C/N,S-C is 56 mV dec^{-1} , which is smaller than that of the Mo₂C/S-C (75 mV dec^{-1}) and the c-Mo₂C (110 mV dec^{-1}), thereby suggesting the occurrence of the Volmer–Heyrovsky mechanism along with the faster HER kinetics in the Mo₂C/N,S-C.

The Nyquist plots obtained from the electrochemical impedance spectroscopy (EIS) of the catalysts are presented in Figure 3c, where the charge transfer resistance (R_{ct}) at the electrode and electrolyte interface is represented by a semicircle and is inversely proportional to the electrocatalytic activity [20,44]. The R_{ct} value of Mo₂C/N,S-C (12.4Ω), which is smaller than that of Mo₂C/S-C (35.1Ω) and c-Mo₂C (200Ω), thereby implies rapid electron transfer and improved HER activity.

The cyclic voltammogram (CV) curves of the catalysts in the non-faradaic region are provided in Figure S5a–c, and the corresponding double-layer capacitance (C_{dl}) values

are shown in Figure S5d. The Mo₂C/N,S-C catalysts exhibited a higher C_{dl} value of 18.02 mF cm⁻² than Mo₂C/S-C (5.47 mF cm⁻²) and Mo₂C (1.34 mF cm⁻²). In general, C_{dl} is proportional to the contact area between catalyst and electrolyte. Accordingly, the contact area of Mo₂C/N,S-C is larger than other catalysts, which additionally contributes to the higher HER activity [25].

The polarization curves of the Mo₂C/N,S-C obtained before and after 3000 cycles between 0.2 and -0.2 V (vs. RHE) are presented in Figure 3d. This reveals the good stability of the catalyst in alkaline media, with little change in the polarization curve, and a marginal increase in the η₁₀ value from 105 to 117 mV, after 3000 cycles. Since durability is a significant factor in determining the HER performance, the highly active and durable Mo₂C/N,S-C has clear potential as a HER electrocatalyst.

4. Conclusions

In summary, a simple and environmentally friendly method to produce Mo₂C nanoparticles dispersed onto N,S co-doped carbon scaffold was designed by using the lignosulfonate, an industrial waste material. The as-prepared Mo₂C/N,S-C catalyst exhibited a high HER performance with a small η₁₀ value of 105 mV and a good stability for 3000 cycles. The improved HER performance resulted from a synergy between the highly active Mo₂C nanoparticles and N,S co-doped carbon scaffold, thus providing high electrical conductivity and large surface area. Compared to solely doped carbon scaffolds, N,S-C scaffold can further enhance the HER performance of Mo₂C by adjusting the catalytic activity of carbon atoms adjacent to heteroatoms. In addition, N,S co-doping to carbon modulated the hydrophilicity of the catalyst surface, thereby further enhancing the HER activity. Thus, considering this simple and environmentally friendly method, the proposed Mo₂C/N,S-C could be a promising HER catalyst with a high activity and stability.

Supplementary Materials: The following supporting information can be downloaded at: <https://www.mdpi.com/article/10.3390/nano12173047/s1>, Figure S1: (a) TEM and (b) HR-TEM images for Mo₂C/S-C; Figure S2: XPS survey scan of Mo₂C/N,S-C; Figure S3: XPS spectra of Mo₂C/S-C. (a) Survey, (b) Mo 3d (c) N 1s, and (d) S 2p; Figure S4: (a) N₂-sorption isotherm and (b) pore size distribution of Mo₂C/N,S-C; Figure S5: CV graphs of (a) Mo₂C/N,S-C, (b) Mo₂C/S-C and (c) Mo₂C measured at scan rates from 20 to 180 mV s⁻¹ between potential range of 0.1 and 0.3 V (vs. RHE) in 1 M KOH. (d) measured capacitive currents at 0.2 V (vs. RHE) as a function of scan rate; Table S1: Element contents of lignosulfonate; Table S2: The amounts of each element for Mo₂C/N,S-C and Mo₂C/S-C; Table S3: Comparison of HER performance in alkaline media with various reported biomass-derived molybdenum carbide-based catalysts. References [45–53].

Author Contributions: Conceptualization, Y.S.K. and D.H.Y.; methodology, N.Y.O. and D.H.Y.; validation, Y.S.K. and D.H.Y.; formal analysis, N.Y.O.; investigation, N.Y.O., S.Y.P. and J.Y.H.; resources, Y.S.K. and D.H.Y.; data curation, N.Y.O., S.Y.P., J.Y.H. and H.M.J.; writing—original draft preparation, N.Y.O., S.Y.P., J.Y.H., H.M.J., Y.S.K. and D.H.Y.; writing—review and editing, N.Y.O. and D.H.Y.; visualization, N.Y.O. and D.H.Y.; supervision, D.H.Y.; project administration, Y.S.K. and D.H.Y.; funding acquisition, Y.S.K. and D.H.Y. All authors have read and agreed to the published version of the manuscript.

Funding: This study was carried out with the support of the R&D Program for Forest Science Technology (FTIS2020216B10-2222-AC01) provided by the Korea Forest Service (Korea Forestry Promotion Institute) and the National Research Foundation of Korea (NRF) grant funded by the Korean government (Ministry of Education) (2019R1I1A3A01052741). This work was also supported by the Korean Institute of Energy Technology Evaluation and Planning (KETEP) and the Ministry of Trade, Industry & Energy (MOTIE) of the Republic of Korea (No. 20224000000080).

Institutional Review Board Statement: Not applicable.

Informed Consent Statement: Not applicable.

Data Availability Statement: All data is contained within the article.

Acknowledgments: The central laboratory of Kangwon National University and Korea Basic Science Institute (Chuncheon) provided significant assistance with the TEM analyses.

Conflicts of Interest: The authors declare no conflict of interest.

References

1. Yu, Z.-Y.; Duan, Y.; Feng, X.-Y.; Yu, X.; Gao, M.-R.; Yu, S.-H. Clean and affordable hydrogen fuel from alkaline water splitting: Past, recent progress, and future prospects. *Adv. Mater.* **2021**, *33*, 2007100. [\[CrossRef\]](#)
2. Dresselhaus, M.S.; Thomas, I.L. Alternative energy technologies. *Nature* **2001**, *414*, 332–337. [\[CrossRef\]](#)
3. Lin, Z.; Xiao, B.; Huang, M.; Yan, L.; Wang, Z.; Huang, Y.; Shen, S.; Zhang, Q.; Gu, L.; Zhong, W. Realizing negatively charged metal atoms through controllable d-electron transfer in ternary Ir_{1-x}Rh_xSb intermetallic alloy for hydrogen evolution reaction. *Adv. Energy Mater.* **2022**, *12*, 2200855. [\[CrossRef\]](#)
4. Buttler, A.; Spliethoff, H. Current status of water electrolysis for energy storage, grid balancing and sector coupling via power-to-gas and power-to-liquids: A review. *Renew. Sust. Energ. Rev.* **2018**, *82*, 2440–2454. [\[CrossRef\]](#)
5. Kim, J.Y.; Magesh, G.; Youn, D.H.; Jang, J.-W.; Kubota, J.; Domen, K.; Lee, J.S. Single-crystalline, wormlike hematite photoanodes for efficient solar water splitting. *Sci. Rep.* **2013**, *3*, 2681. [\[CrossRef\]](#)
6. Sheng, W.; Myint, M.; Chen, J.G.; Yan, Y. Correlating the hydrogen evolution reaction activity in alkaline electrolytes with the hydrogen binding energy on monometallic surfaces. *Energy Environ. Sci.* **2013**, *6*, 1509–1512. [\[CrossRef\]](#)
7. Wang, J.; Xu, F.; Jin, H.; Chen, Y.; Wang, Y. Non-noble metal-based carbon composites in hydrogen evolution reaction: Fundamentals to applications. *Adv. Mater.* **2017**, *29*, 1605838. [\[CrossRef\]](#)
8. Tang, C.; Zhang, R.; Lu, W.; Wang, Z.; Liu, D.; Hao, S.; Du, G.; Asiri, A.M.; Sun, X. Energy-saving electrolytic hydrogen generation: Ni₂P nanoarray as a high-performance non-noble-metal electrocatalyst. *Angew. Chem. Int. Ed.* **2017**, *56*, 842–846. [\[CrossRef\]](#)
9. Wu, C.; Li, J. Unique hierarchical Mo₂C/C nanosheet hybrids as active electrocatalyst for hydrogen evolution reaction. *ACS Appl. Mater. Interfaces* **2017**, *9*, 41314–41322. [\[CrossRef\]](#)
10. Ge, C.; Jiang, P.; Cui, W.; Pu, Z.; Xing, Z.; Asiri, A.M.; Obaid, A.Y.; Sun, X.; Tian, J. Shape-controllable synthesis of Mo₂C nanostructures as hydrogen evolution reaction electrocatalysts with high activity. *Electrochim. Acta* **2014**, *134*, 182–186. [\[CrossRef\]](#)
11. Youn, D.H.; Jang, J.-W.; Kim, J.Y.; Jang, J.S.; Choi, S.H.; Lee, J.S. Fabrication of graphene-based electrode in less than a minute through hybrid microwave annealing. *Sci. Rep.* **2014**, *4*, 5492. [\[CrossRef\]](#)
12. Voiry, D.; Salehi, M.; Silva, R.; Fujita, T.; Chen, M.; Asefa, T.; Shenoy, V.B.; Eda, G.; Chhowalla, M. Conducting MoS₂ nanosheets as catalysts for hydrogen evolution reaction. *Nano Lett.* **2013**, *13*, 6222–6227. [\[CrossRef\]](#)
13. Xie, J.; Li, S.; Zhang, X.; Zhang, J.; Wang, R.; Zhang, H.; Pan, B.; Xie, Y. Atomically-thin molybdenum nitride nanosheets with exposed active surface sites for efficient hydrogen evolution. *Chem. Sci.* **2014**, *5*, 4615–4620. [\[CrossRef\]](#)
14. Park, S.H.; Jo, T.H.; Lee, M.H.; Kawashima, K.; Mullins, C.B.; Lim, H.-K.; Youn, D.H. Highly active and stable nickel-molybdenum nitride (Ni₂Mo₃N) electrocatalyst for hydrogen evolution. *J. Mater. Chem. A* **2021**, *9*, 4945–4951. [\[CrossRef\]](#)
15. Lee, M.H.; Youn, D.H.; Lee, J.S. Nanostructured molybdenum phosphide/N-doped carbon nanotube-graphene composites as efficient electrocatalysts for hydrogen evolution reaction. *Appl. Catal. A Gen.* **2020**, *594*, 117451. [\[CrossRef\]](#)
16. Miao, M.; Pan, J.; He, T.; Yan, Y.; Xia, B.Y.; Wang, X. Molybdenum carbide-based electrocatalysts for hydrogen evolution reaction. *Chem. Eur. J.* **2017**, *23*, 10947–10961. [\[CrossRef\]](#)
17. Wan, C.; Regmi, Y.N.; Leonard, B.M. Multiple phases of molybdenum carbide as electrocatalysts for the hydrogen evolution reaction. *Angew. Chem. Int. Ed.* **2014**, *53*, 6407–6410. [\[CrossRef\]](#)
18. Vrabel, H.; Hu, X. Molybdenum boride and carbide catalyze hydrogen evolution in both acidic and basic solutions. *Angew. Chem. Int. Ed.* **2012**, *51*, 12703–12706. [\[CrossRef\]](#)
19. Ma, Y.; Guan, G.; Hao, X.; Cao, J.; Abudula, A. Molybdenum carbide as alternative catalyst for hydrogen production—A review. *Renew. Sust. Energ. Rev.* **2017**, *75*, 1101–1129. [\[CrossRef\]](#)
20. Jing, S.; Zhang, L.; Luo, L.; Lu, J.; Yin, S.; Shen, P.K.; Tsiakaras, P. N-doped porous molybdenum carbide nanobelts as efficient catalysts for hydrogen evolution reaction. *Appl. Catal. B* **2018**, *224*, 533–540. [\[CrossRef\]](#)
21. Li, J.-S.; Wang, Y.; Liu, C.-H.; Li, S.-L.; Wang, Y.-G.; Dong, L.-Z.; Dai, Z.-H.; Li, Y.-F.; Lan, Y.-Q. Coupled molybdenum carbide and reduced graphene oxide electrocatalysts for efficient hydrogen evolution. *Nat. Commun.* **2016**, *7*, 11204. [\[CrossRef\]](#)
22. He, C.; Tao, J. Synthesis of nanostructured clean surface molybdenum carbides on graphene sheets as efficient and stable hydrogen evolution reaction catalysts. *Chem. Commun.* **2015**, *51*, 8323–8325. [\[CrossRef\]](#) [\[PubMed\]](#)
23. Lee, G.H.; Lee, M.H.; Kim, Y.; Lim, H.-K.; Youn, D.H. Facile synthesis of nanostructured molybdenum carbide/nitrogen-doped CNT-RGO composite via a modified urea glass route for efficient hydrogen evolution. *J. Alloys Compd.* **2019**, *805*, 113–119. [\[CrossRef\]](#)
24. Liu, Y.; Yu, G.; Li, G.D.; Sun, Y.; Asefa, T.; Chen, W.; Zou, X. Coupling Mo₂C with nitrogen-rich nanocarbon leads to efficient hydrogen-evolution electrocatalytic sites. *Angew. Chem. Int. Ed.* **2015**, *54*, 10752–10757. [\[CrossRef\]](#)
25. Jo, H.M.; Kim, Y.; Youn, D.H. One-pot synthesis of molybdenum carbide/N-doped carbon nanotube composite using nitrilotriacetic acid for efficient hydrogen evolution. *J. Alloys Compd.* **2021**, *855*, 157420. [\[CrossRef\]](#)

26. Oh, N.Y.; Lee, G.H.; Jeong, H.M.; Kim, Y.S.; Youn, D.H. Kraft lignin derived molybdenum carbide/nitrogen-doped carbon composite for efficient hydrogen evolution reaction. *J. Electrochem. Soc.* **2021**, *168*, 084511. [[CrossRef](#)]
27. Vanholme, R.; Demedts, B.; Morreel, K.; Ralph, J.; Boerjan, W. Lignin biosynthesis and structure. *Plant Physiol.* **2010**, *153*, 895–905. [[CrossRef](#)]
28. Chio, C.; Sain, M.; Qin, W. Lignin utilization: A review of lignin depolymerization from various aspects. *Renew. Sust. Energ. Rev.* **2019**, *107*, 232–249. [[CrossRef](#)]
29. Mansouri, N.-E.E.; Salvadó, J. Structural characterization of technical lignins for the production of adhesives: Application to lignosulfonate, kraft, soda-anthraquinone, organosolv and ethanol process lignins. *Ind. Crops Prod.* **2006**, *24*, 8–16. [[CrossRef](#)]
30. Jeon, J.; Yoo, J.-K.; Yim, S.; Jeon, K.; Lee, G.H.; Yun, J.H.; Kim, D.K.; Jung, Y.S. Natural-wood-derived lignosulfonate ionomer as multifunctional binder for high-performance lithium–sulfur battery. *ACS Sustain. Chem. Eng.* **2019**, *7*, 17580–17586. [[CrossRef](#)]
31. Rinaldi, R.; Jastrzebski, R.; Clough, M.T.; Ralph, J.; Kennema, M.; Bruijninx, P.C.A.; Weckhuysen, B.M. Paving the way for lignin valorisation: Recent advances in bioengineering, biorefining and catalysis. *Angew. Chem. Int. Ed.* **2016**, *55*, 8164–8215. [[CrossRef](#)] [[PubMed](#)]
32. Brainard, W.A.; Wheeler, D.R. An XPS study of the adherence of refractory carbide silicide and boride rf-sputtered wear-resistant coatings. *J. Vac. Sci. Technol. B* **1978**, *15*, 1800–1805. [[CrossRef](#)]
33. Sarma, D.D.; Rao, C.N.R. XPS studies of oxides of second- and third-row transition metals including rare earths. *J. Electron. Spectrosc. Relat. Phenom.* **1980**, *20*, 25–45. [[CrossRef](#)]
34. Jones, R.; Adams, J.M.; Evans, S. A new barium molybdate phase. *Mater. Res. Bull.* **1987**, *22*, 351–358. [[CrossRef](#)]
35. Zhou, Y.; Leng, Y.; Zhou, W.; Huang, J.; Zhao, M.; Zhan, J.; Feng, C.; Tang, Z.; Chen, S.; Liu, H. Sulfur and nitrogen self-doped carbon nanosheets derived from peanut root nodules as high-efficiency non-metal electrocatalyst for hydrogen evolution reaction. *Nano Energy* **2015**, *16*, 357–366. [[CrossRef](#)]
36. Huang, Y.; Candelaria, S.L.; Li, Y.; Li, Z.; Tian, J.; Zhang, L.; Cao, G. Sulfurized activated carbon for high energy density supercapacitors. *J. Power Sources* **2014**, *252*, 90–97. [[CrossRef](#)]
37. Liang, J.; Jiao, Y.; Jaroniec, M.; Qiao, S.Z. Sulfur and nitrogen dual-doped mesoporous graphene electrocatalyst for oxygen reduction with synergistically enhanced performance. *Angew. Chem. Int. Ed.* **2012**, *51*, 11496–11500. [[CrossRef](#)]
38. Wang, Q.; Yu, R.; Shen, D.; Liu, G.; Luo, K.H.; Wu, C.; Gu, S. One-pot synthesis of Mo₂C&MoS₂ loaded on N/S co-doped carbon materials as the electrocatalysts for hydrogen evolution reaction. *Fuel* **2022**, *318*, 123615.
39. Tan, H.; Liu, J.; Huang, G.; Qian, Y.; Deng, Y.; Chen, G. Understanding the roles of sulfur doping for enhancing of hydrophilicity and electrochemical performance of N,S-codoped hierarchically porous carbon. *ACS Appl. Energy Mater.* **2018**, *1*, 5599–5608. [[CrossRef](#)]
40. Zhao, J.; Lai, H.; Lyu, Z.; Jiang, Y.; Xie, K.; Wang, X.; Wu, Q.; Yang, L.; Jin, Z.; Ma, Y.; et al. Hydrophilic hierarchical nitrogen-doped carbon nanocages for ultrahigh supercapacitive performance. *Adv. Mater.* **2015**, *27*, 3541–3545. [[CrossRef](#)]
41. Zhang, J.; Zhang, M.; Zeng, Y.; Chen, J.; Qiu, L.; Zhou, H.; Sun, C.; Yu, Y.; Zhu, C.; Zhu, Z. Single Fe atom on hierarchically porous S, N-codoped nanocarbon derived from porphyrin enable boosted oxygen catalysis for rechargeable Zn-Air batteries. *Small* **2019**, *15*, 1900307. [[CrossRef](#)]
42. Qi, C.; Ma, X.; Ning, G.; Song, X.; Chen, B.; Lan, X.; Li, Y.; Zhang, X.; Gao, J. Aqueous slurry of S-doped carbon nanotubes as conductive additive for lithium ion batteries. *Carbon* **2015**, *92*, 245–253. [[CrossRef](#)]
43. Ang, H.; Tan, H.T.; Luo, Z.M.; Zhang, Y.; Guo, Y.Y.; Guo, G.; Zhang, H.; Yan, Q. Hydrophilic nitrogen and sulfur co-doped molybdenum carbide nanosheets for electrochemical hydrogen evolution. *Small* **2015**, *11*, 6278–6284. [[CrossRef](#)]
44. Ma, S.; Deng, J.; Xu, Y.; Tao, W.; Wang, X.; Lin, Z.; Zhang, Q.; Gu, L.; Zhong, W. Pollen-like self-supported FeIr alloy for improved hydrogen evolution reaction in acid electrolyte. *J. Energy Chem.* **2022**, *66*, 560–565. [[CrossRef](#)]
45. Guo, T.; Zhang, X.; Liu, T.; Wu, Z.; Wang, D. N, K Co-activated biochar-derived molybdenum carbide as efficient electrocatalysts for hydrogen evolution. *Appl. Surf. Sci.* **2020**, *509*, 144879. [[CrossRef](#)]
46. Kang, Q.; Li, M.; Wang, Z.; Lu, Q.; Gao, F. Agaric-derived N-doped carbon nanorod arrays@nanosheet networks coupled with molybdenum carbide nanoparticles as highly efficient pH-universal hydrogen evolution electrocatalysts. *Nanoscale* **2020**, *12*, 5159–5169. [[CrossRef](#)] [[PubMed](#)]
47. Pu, Z.; Wang, M.; Kou, Z.; Amiin, I.S.; Mu, S. Mo₂C quantum dot embedded chitosan-derived nitrogen-doped carbon for efficient hydrogen evolution in a broad pH range. *Chem. Commun.* **2016**, *52*, 12753–12756. [[CrossRef](#)]
48. Han, W.; Chen, L.; Ma, B.; Wang, J.; Song, W.; Fan, X.; Li, Y.; Zhang, F.; Peng, W. Ultra-small Mo₂C nanodots encapsulated in nitrogen-doped porous carbon for pH-universal hydrogen evolution: Insights into the synergistic enhancement of HER activity by nitrogen doping and structural defects. *J. Mater. Chem.* **2019**, *7*, 4734–4743. [[CrossRef](#)]
49. An, K.; Xu, X. Mo₂C based electrocatalyst with nitrogen doped three-dimensional mesoporous carbon as matrix, synthesis and HER activity study. *Electrochim. Acta* **2019**, *293*, 348–355. [[CrossRef](#)]
50. An, K.; Xu, X.; Liu, X. Mo₂C-based electrocatalyst with biomass-derived sulfur and nitrogen co-doped carbon as a matrix for hydrogen evolution and organic pollutant removal. *ACS Sustain. Chem. Eng.* **2018**, *6*, 1446–1455. [[CrossRef](#)]
51. Wu, Z.-Y.; Hu, B.-C.; Wu, P.; Liang, H.-W.; Yu, Z.-L.; Lin, Y.; Zheng, Y.-R.; Li, Z.; Yu, S.-H. Mo₂C nanoparticles embedded within bacterial cellulose-derived 3D N-doped carbon nanofiber networks for efficient hydrogen evolution. *NPG Asia Mater.* **2016**, *8*, e288. [[CrossRef](#)]

-
52. Kang, Q.; Qin, Y.; Lu, Q.; Gao, F. Waste leather-derived (Cr, N)-co-doped carbon cloth coupling with Mo₂C nanoparticles as a self-supported electrode for highly active hydrogen evolution reaction performances. *J. Power Sources* **2020**, *476*, 228706. [[CrossRef](#)]
 53. Chen, X.; Sun, J.; Guo, T.; Zhao, R.; Liu, L.; Liu, B.; Wang, Y.; Li, J.; Du, J. Biomass-derived carbon nanosheets coupled with MoO₂/Mo₂C electrocatalyst for hydrogen evolution reaction. *Int. J. Hydrogen Energy* **2022**. [[CrossRef](#)]